Far-Field Perfect Imaging with Time-Modulated Gratings

Pawel Packo[1] and Dani Torrent[2,*]

[1] *Department of Robotics and Mechatronics, AGH - University of Science and Technology, Al. A. Mickiewicza 30, Kraków 30-059, Poland*

[2] *GROC, UJI, Institut de Noves Tecnologies de la Imatge (INIT), Universitat Jaume I, Castelló 12071, Spain*

(Received 28 December 2021; revised 5 May 2022; accepted 12 May 2022; published 22 June 2022)

We study the capabilities of time-modulated diffraction gratings as imaging devices. It is shown that a time-dependent but transversally homogeneous slab can be used to make a perfect image of an object in the far-field, since all the evanescent modes couple to propagative time-diffracted orders. It is found that, if the image to be obtained is axially symmetric, it can be recovered by measuring the time signal at a single point, without the need to perform a spatial scan, so that time gratings can act as well as single-pixel imaging devices. In the case of having an object without axial symmetry, the time grating can be combined with a spatial grating, and then the full image can be recovered again with a measurement at a single point. We apply the theory of compressive sensing to optimize the recovery method, and numerical examples are provided. We show, therefore, that time-modulated gratings can be used to perfectly recover the image of an object in the far-field and after measuring at a single point in space, making them a promising approach to superresolution and ultrafast imaging.

DOI: 10.1103/PhysRevApplied.17.064040

The recovery of the image of an object by analyzing the shape of an undulatory field (typically acoustic or electromagnetic) that interacts with it is the usual method for imaging. This method has a limitation imposed by the theory of diffraction, namely, that only details of the order of the wavelength of the field can be coupled to free space. The field carries also information about details finer than the wavelength, but in the form of evanescent waves that exist only in the proximity of the object, so that these can be recovered only in the near-field [1].

In order to overcome the limitations imposed by diffraction, a large number of methods have been proposed, most of which essentially couple these evanescent waves to free propagating waves [2–9], so that the resolution of the image is increased. The underlying idea of these methods consists in enhancing the interaction of evanescent modes with spatially structured objects, so that free propagating waves are excited. However, the resolution of the image is still limited by the finite size of the image-processing system, since the evanescent modes are coupled to free waves traveling in all directions in space. Therefore, in order to fully recover the image of the object we should collect all these waves, which is impossible for a physically finite system.

Due to the ability to spatially manipulate fields, metamaterials [10–12], which are artificial periodic structures especially designed to control optical and acoustical fields, have been widely used to overcome the diffraction limit of conventional imaging systems [6,13–16]. Metamaterials have offered a number of extraordinary applications and recently their "time version," that is, the temporal modulation of the materials' properties instead of their spatial modulation, is receiving increasing attention, since they such as additional properties and applications not achievable by their spatial counterparts, like dynamic control of propagation [17], tunability [18], nonreciprocity [19–22], and gain [23].

In this work we show that a time-modulated surface can be used to couple evanescent modes to free space, so that this concept can be used to overcome the diffraction limit of conventional imaging systems. In the same way that a spatial grating excites a set of diffracted modes traveling in different directions, a time grating excites a set of waves at different frequencies, each of which carries information about the Fourier transform of the image we want to recover. It will be shown that we can recover the image of the object either by analyzing the fundamental of these frequencies and make a spatial scan, or by analyzing the temporal spectrum at a single point in space, showing that time gratings can be used for ultrafast and single-pixel imaging devices.

*dtorrent@uji.es

I. TIME GRATINGS AS DYNAMIC SPATIAL FIELD MODULATORS

Our model equation will be the scalar wave equation in free space,

$$\nabla^2\psi = \frac{1}{c_0^2}\partial_{tt}\psi, \tag{1}$$

where c_0 is the phase speed of the wave field ψ.

The time grating is modeled as an infinitesimally thin impedance boundary whose response is time-dependent; consequently, the field will be continuous at this interface while the normal component of the derivative will have a step discontinuity [24] given by

$$\partial_z\psi^+ - \partial_z\psi^- = \xi(t)\psi \quad \text{at } z = 0, \tag{2}$$

where ξ is the time-modulated impedance of the surface and $\pm$ indicates the field ψ at $z = 0^{\pm}$. We assume that the impedance is temporally modulated with repetition frequency ν, so that we can expand $\xi(t)$ as a Fourier series,

$$\xi(t) = \sum_{n=-\infty}^{\infty} \xi_n e^{-i2\pi n\nu t}. \tag{3}$$

Let us assume that a plane wave of unit amplitude with transverse (grating-in-plane) wavevector $\mathbf{k}$ and frequency ω_0 arrives at the grating, as shown in Fig. 1(a). The solution for the field $\psi(z,t)$ will be given by

$$\psi(z,t) = e^{iq_0 z}e^{-i\omega_0 t} + \sum_n C_n e^{\pm iq_n z}e^{-i\Omega_n t}, \tag{4}$$

where $q_n = \sqrt{\Omega_n^2/c_0^2 - k^2}$ (with $k = |\mathbf{k}|$) and $\Omega_n = \omega_0 + 2n\pi\nu$. The $\pm$ in (4) refers to either $z > 0$ or $z < 0$. The above solution already satisfies the field continuity condition, while the discontinuity of the derivative condition, after using (4) in (2), yields

$$2iq_n C_n = \sum_m \xi_{n-m}(\delta_{m0} + C_m), \tag{5}$$

so that we can solve for the C_m coefficients from the system of equations

$$\sum_m (2iq_n\delta_{nm} - \xi_{n-m})C_m = \xi_n. \tag{6}$$

The field behind the impedance plane (i.e., $z > 0$) will be composed of a set of diffracted waves with amplitudes

$$T_n = \delta_{n0} + C_n. \tag{7}$$

Therefore, the periodic temporal modulation of the impedance of the surface excites a set of diffracted waves in a similar way to the periodic spatial modulation, and it behaves as a diffraction grating. It is clearly an "active" grating in the sense that energy is not conserved in this process, since the time-dependence in the parameters of the grating has to be induced externally, and some energy has to be supplied to the system [23].

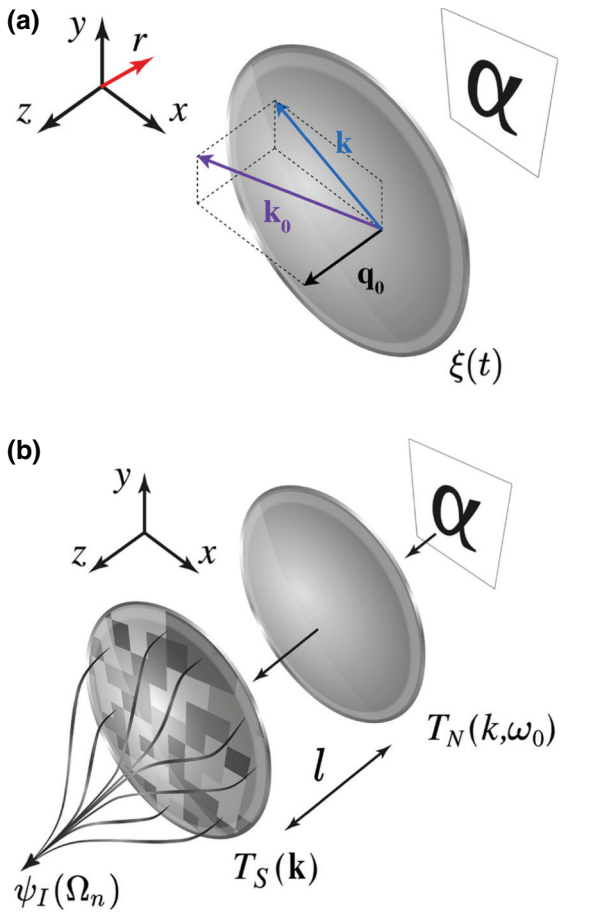

FIG. 1. (a) Setup for imaging with a homogeneous time-modulated grating. (b) Setup for single-pixel imaging with a time-modulated grating combined with a second grating which can be identical to the first one or a random time-invariant receiving screen, depending on the application.

The above equations have been derived assuming that the incident field is a monochromatic plane wave of unitary amplitude. In more generic cases, the incident field will be made up by a linear combination of plane waves of the form [1],

$$\psi_0(\mathbf{r},t) = \iint A_0(\mathbf{k})e^{i\mathbf{k}\cdot\mathbf{r}}e^{iq_0 z}e^{-i\omega_0 t}d^2\mathbf{k}, \tag{8}$$

where $\mathbf{r}$ is a two-dimensional (2D) vector defined in the x–y plane. The transmitted field will be

$$\psi_T(\mathbf{r},t) = \sum_n \iint A_0(\mathbf{k})T_n(k,\omega_0)e^{i\mathbf{k}\cdot\mathbf{r}}e^{-i\Omega_n t}d^2\mathbf{k}, \tag{9}$$

which can be expressed as

$$\psi_T(\mathbf{r},t) = \sum_n e^{-i\Omega_n t} \iint A_0(\mathbf{r}') T_n(\mathbf{r},\mathbf{r}') d^2\mathbf{r}', \tag{10}$$

with

$$T_n(\mathbf{r},\mathbf{r}') = \iint T_n(k,\omega_0) e^{i\mathbf{k}\cdot(\mathbf{r}-\mathbf{r}')} d^2\mathbf{k}. \tag{11}$$

It can therefore be seen that the role of the grating is to generate an infinite set of harmonics whose field distributions are different, since the transmittance of the grating is different for each harmonic. Interestingly, this is equivalent to saying that the grating behaves as a spatial light modulator if the field comprises optical waves or a spatial field modulator in the most general case. Spatial light modulators have been widely used in optics for many applications; however, they need to be spatially modified. In this case, we modulate a signal by a grating and send the harmonics at once with all the possible patterns. We will see later how this effect can be exploited to recover the image of an object after measuring at a single point.

Although the above problem is scalar, the fundamental principles described by it will apply as well to vectorial waves (e.g., elastic or electromagnetic). The main difference will be the calculation of the transmission and reflection coefficients by the grating, due to the different definitions of the impedance boundary, but it is obvious that the principles of diffraction and imaging, as explained before, will be identical. Consequently, we limit the study to the scalar wave equation, while bearing in mind that the results presented here will be very similar for vectorial waves.

II. FAR-FIELD IMAGING WITH A TIME GRATING

Let us now suppose that we want to recover the image of an object illuminated by a plane wave of frequency ω_0. We define the image as a 2D screen such that just after the screen the field distribution is $\psi_0(\mathbf{r}, z = 0)$, so that a set of plane waves whose amplitudes can be obtained from the Fourier transform $A_0(\mathbf{k})$ of $\psi_0(\mathbf{r}, z = 0)$ is propagating along the z axis. However, for those wave numbers such that $k > k_0$ the propagation along z is evanescent, since q_0 is a complex number. Consequently, the information carried by the amplitude $A_0(\mathbf{k})$ for these wave numbers ($k > k_0$) exists only in the near-field and will be lost upon propagation; therefore, we will not be able to fully recover the image at a certain (rather small) distance from the source.

We can avoid this loss of information by putting a time grating just after the object at $z = 0$. The grating's response $T_n(k)$ depends on ω_0, omitted for simplicity, as well as on the wave number modulus k, since at the moment we assume the grating is homogeneous (i.e. its impedance does not depend on position) and it cannot distinguish an image from its rotated version. However, the response of the grating implies that for all $\mathbf{k}$ there will always be a diffraction order n such that q_n will be real and, consequently, the information carried by $A_0(\mathbf{k})$ will not be lost at any distance from the source. Therefore, higher harmonics are responsible for passing higher ks beyond the imaging grating as propagating modes, up to physical constraints related to attenuation of the wave components in a practical realization of the system.

For the recovery of the image, a "mirror-grating" configuration is used. The fundamental idea is illustrated in Fig. 1(b), where an identical [i.e. $T_S(\mathbf{k}) = T_n(k,\omega_0)$] mirror grating, placed at a distance l from the object and the imaging grating, is used as a recovery system, since it will couple all the information of the object into the fundamental component of the field. Then, after the mirror grating, we will have

$$\psi_I(\mathbf{r},t) = \sum_{m=-\infty}^{\infty} e^{-i\Omega_m t} \iint B_m(\mathbf{k}) e^{i\mathbf{k}\cdot\mathbf{r}} d^2\mathbf{k}, \tag{12}$$

with

$$B_m(\mathbf{k}) = A_0(\mathbf{k}) \sum_{n=-\infty}^{\infty} T_n(k) T_{m-n}(k) e^{iq_n l}, \tag{13}$$

where only the terms for which q_n is real will be relevant for the sum. Thus, if we measure the spatial field distribution corresponding to the source frequency ω_0 and perform its spatial Fourier transform we obtain the $B_0(\mathbf{k})$ coefficients from which we can retrieve the source's Fourier transform from the above equation for $m = 0$.

To fully recover the image the condition is that we are able to excite a large enough number of temporal harmonics to propagate the maximum wave number $k_{\max}$, but as long as this happens we will have all the information in the fundamental mode at the mirror grating, with no need for the spatial analysis of higher harmonics. It is important to note that with this configuration we only need to excite higher harmonics at the first grating, not to detect them at the mirror screen, so that perfect imaging can be done by the analysis of the field at the original frequency ω_0 only.

We demonstrate the application of the proposed method with the following example. Assuming unit field frequency, $\omega_0 = 1$ rad/s, and $c_0 = 1$ m/s, we generate real-valued time-modulation signals with the desired number of harmonics with their amplitudes and phases described by complex numbers randomly generated from the uniform distribution, $|\xi_{|n|}| \sim U(0,1)$ and $\angle\xi_{|n|} \sim U(0,2\pi)$. The maximum wave numbers for waves transmitted through the imaging system for modulation signals that excite two and eight harmonics, for two modulation frequencies [$f_0/2$

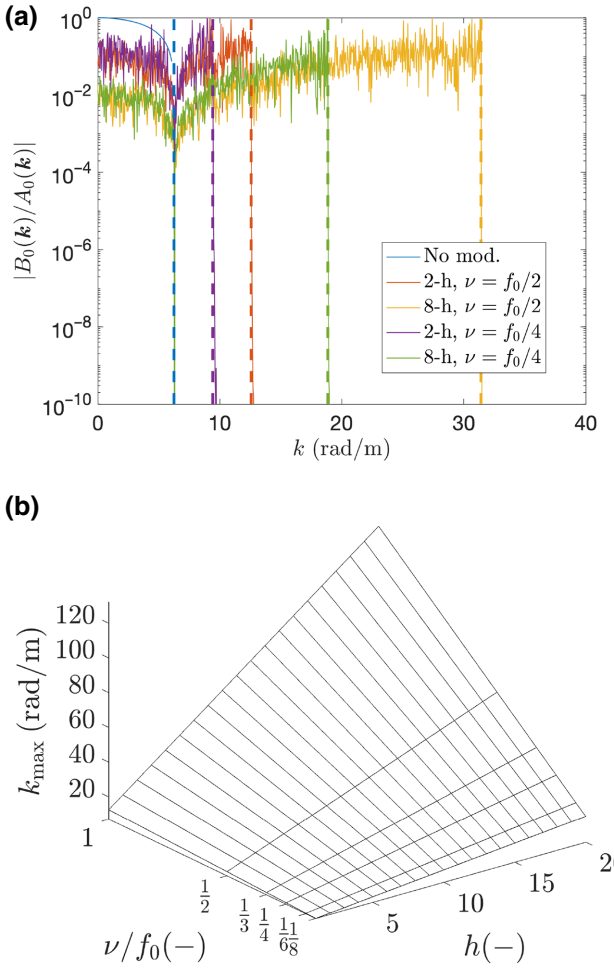

FIG. 2. (a) The ratio $|B_0(\mathbf{k})/A_0(\mathbf{k})|$ [see Eq. (13)] for the field frequency $\omega_0 = 1$ rad/s and modulation frequencies $f_0/2$ and $f_0/4$ and for two and eight excited higher harmonics. Vertical lines show corresponding cut-off wave numbers $k_{\max}$. (b) Maximum wave numbers $k_{\max}$ transferred through the grating system as a function of number of excited harmonics h and modulation frequency ν [$f_0 = \omega_0/(2\pi)$].

and $f_0/4$; $f_0 = \omega_0/(2\pi)$] are illustrated in Fig. 2(a). It can further be seen from Fig. 2(b) that the maximum wave number to be transmitted is a bilinear function of the modulation frequency and the number of harmonics excited by the modulation signal, $k_{\max}(\nu, h)$. Therefore, it is preferred to use high modulation frequencies and/or detect a possibly large number of harmonics in order to increase the quality of image reconstruction.

In order to illustrate how the maximum wave number, $k_{\max}$, enhanced by the imaging with time-modulated gratings, influences image reconstruction we show in Fig. 3 an example letter that will be processed through the proposed system. Assuming that the object is illuminated by a field of unit frequency $\omega_0 = 1$ rad/s propagating at $c_0 = 1$ m/s, the letter is spatially Fourier-transformed and its spectrum truncated to contain wavevectors only up to

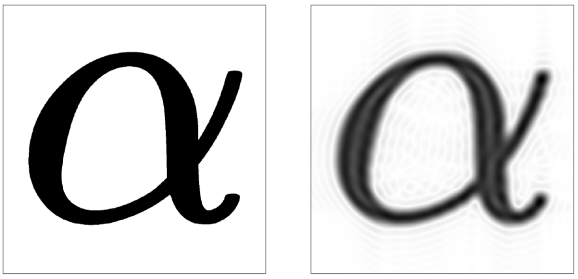

FIG. 3. The model letter α used in numerical experiments (a), and its representation with $(1 + 128) \times (1 + 128)$ samples in the Fourier spectrum (b).

$k_{\max}$ corresponding to a given modulation signal [eight harmonics for $f_0/4$ and $f_0/2$ modulation frequencies, corresponding to Fig. 2(a)]. The reconstruction process consists of inverse Fourier transformation of the truncated spectrum. The results are presented in Fig. 4 for the same letters α assuming their physical dimensions of $\lambda \times \lambda$ (top row of Fig. 4) and $4\lambda \times 4\lambda$ (bottom row of Fig. 4), $\lambda = c_0/f_0$. It is clear that for a letter size equal to the wavelength and no modulation, the reconstructed image does not reveal any features of the original pattern. For only eight harmonics in the signal, however, and relatively low modulation frequencies, the shape of α can be clearly distinguished, especially for $\nu = f_0/2$. When the wavelength is four times smaller (bottom row of Fig. 4), the letter is distinguishable for no modulation and almost perfectly reconstructed with eight harmonics and modulation frequency $\nu = f_0/2$.

III. SINGLE-DETECTOR IMAGING WITH TIME GRATINGS

The time grating allows an additional way to recover the image without performing such a spatial scan. This involves using all the other harmonics Ω_n to obtain spatial

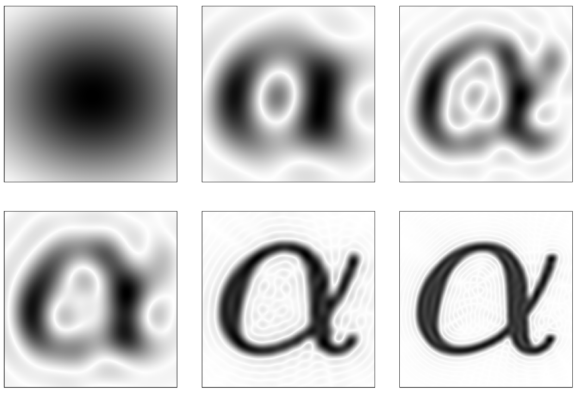

FIG. 4. Recovered images of the letter (from left to right) obtained for $k_{\max}$ for no modulation (left column) and eight harmonics with $\nu = \{f_0/4, f_0/2\}$ (middle and right columns) for image size $\lambda \times \lambda$ (top row) and $4\lambda \times 4\lambda$ (bottom row).

information from the object without scanning the sample. The transversally homogeneous nature of the time grating (the impedance uniformly distributed in space) does not allow different orientations of the image to be distinguished, but the second grating can be replaced by an inhomogeneous receiving screen of transmittance $T_S(\mathbf{r})$. The total field after this screen can be collected and integrated, so that a single time-dependent signal is received, as illustrated in Fig. 1(b). If we measure the spectrum of this integrated signal, we will observe peaks at the different harmonics Ω_n. Then the field distribution of the nth harmonic after this screen will be

$$\psi_I(\Omega_n) = \iint d^2\mathbf{r} T_S(\mathbf{r}) \iint A_0(\mathbf{k}) T_n(k,\omega_0) e^{i\mathbf{k}\cdot\mathbf{r}} e^{iq_n l} d^2\mathbf{k}, \tag{14}$$

which is equivalent to

$$\psi_I(\Omega_n) = \iint T_S^*(\mathbf{k}) T_n(k,\omega_0) e^{iq_n l} A_0(\mathbf{k}) d^2\mathbf{k}, \tag{15}$$

where $T_S(\mathbf{k})$ is the Fourier transform of the transmittance of the screen. The above equation can be seen as a linear system of equations of the form

$$y_n = \sum_m M_{nm} A_m, \tag{16}$$

where the y_n are the measurement points $\psi_I(\Omega_n)$ (amplitudes and phases of harmonics) and A_m are the unknown coefficients $A_0(\mathbf{k})$, which have been discretized into a set of $\mathbf{k}_m$ elements and ordered in a vector labeled by m. Similarly, the matrix M_{nm} is defined as

$$M_{nm} = T_n(k_m,\omega_0) T_S^*(\mathbf{k}_m) e^{iq_n l}, \tag{17}$$

and the knowledge of this matrix will allow us to recover all the A_m from the spectrum of a signal received in a single detector. This approach is similar to single-pixel imaging methods, with the notable difference that all the information is encoded in different harmonics. A possibly large number of harmonics is required in order to fully recover the components of $A_0(\mathbf{k}_m)$. It is known, however, that images are sparse in the $\mathbf{k}$ space, hence large $k_{\max}$ does not in general mean that a large n in Eq. (16) is necessary. Also, it has to be pointed out that the screen S should not have any inversion symmetry, since this would imply the column vectors of M_{nm} corresponding to $\mathbf{k}$ and $-\mathbf{k}$ are identical and, consequently, the matrix M_{nm} would not be invertible. The latter is indeed why the second receiving screen is required to recover the image from one single measurement. Note that since the time-modulated grating is homogeneous in space, only axially symmetric images could be recovered. Also, since the time grating is modulated externally, in the case of not having enough harmonics to recover the image, the modulation pattern (coding sequence) can be changed and the size of both the measurement set y_n and the matrix M_{nm} may be increased, since the T_n elements will depend on the shape of the modulation.

Finally, it must be pointed out that the exponential term in Eq. (17) may vanish for $q_n = \sqrt{k_n^2 - k^2}$, $k_n = \sqrt{\Omega_n^2/c_0^2} < k$, that is, for small $\Omega_n = \omega_0 + 2\pi n\nu$. Then, clearly, for a modulating frequency being an rth integer multiple of ω_0, we have $\Omega_n = 0$ for $n = -r$ and, consequently, $q_n = ik$ and $e^{iq_n l} = e^{-kl}$. For practical setups, the latter exponential vanishes, lowering the rank of M_{nm}. It may be also concluded that higher and incommensurate (with ω_0) modulation frequencies are favorable for the coding sequences.

Below we present two approaches for recovering the image from the proposed single-pixel imaging system: direct image recovery by directly solving the system (16) and a compressive sensing-based recovery using optimization. In both cases we use an inhomogeneous receiving screen with real-only impedance randomly distributed uniformly in space. The coding sequences are real-valued time-modulation signals of (3), where 16 harmonics ($n = \{0, 1, \ldots, 15\}$) are used and their amplitudes and phases are described by complex numbers randomly generated from the uniform distribution, $|\xi_{|n|}| \sim U(0,1)$ and $\angle\xi_{|n|} \sim U(0, 2\pi)$.

We denote by a single measurement a procedure consisting of sending an input modulating sequence through the system and acquiring the temporal Fourier spectrum of the response consisting of all signals integrated after passing the receiving screen. From this spectrum, a total of 31 harmonics (amplitudes and phases; n rows of M_{nm} matrix) are acquired and stored as a column of M_{nm}. Then the procedure is repeated for another coding sequence and another column is appended to M_{nm}.

In numerical experiments reported in this section, we consider an image of a letter illustrated in the left panel of Fig. 3, of size 1024×1024 pixels. The physical dimension of the letter panel is $\lambda \times \lambda$. For recovery, we use a limited part of the 2D Fourier spectrum of the letter consisting of $(1 + 128) \times (1 + 128)$ samples (corresponding to dc and ± 64 samples in each direction). The letter reconstructed by using all 129×129 samples in the truncated spectrum is presented in the right panel of Fig. 3. Due to the symmetry of the spectrum, the letter is uniquely defined by 8385 complex coefficients A_m.

A. Direct image recovery

For the direct recovery of the image we require the matrix M_{nm} to be square and invertible to recover $A_0, \ldots, A_m$ coefficients. Consequently, a possibly large number of harmonics and a substantial number of measurements will be necessary. We consider 15 harmonics, $n =$

$\{1, \ldots, 15\}$, and take 560 measurements obtaining square M_{nm} and the measurement vector y_n. Through the standard Gauss elimination process we compute A_m from (16). The resulting recovered image of the letter is shown in the bottom right end panel of Fig. 6. The reconstruction process is lossless for the direct recovery.

B. Compressive sensing of the image

The direct recovery of the image requires a number of measurements to be taken before the problem in (16) can be solved. Although the process is relatively simple and fast, the number of measurements can be substantially reduced due to the sparsity of the image in the wave number domain. The sparsity of the example letter α used in the reconstruction can be clearly verified by inspecting Fig. 5, where the letter was reconstructed only from a very limited number of the most significant samples (highest $|A_m|$) in $\mathbf{k}$ space.

For signals having sparse representation in some space (the Fourier space in this case) as A_m, the compressive sensing theory [25] can be used to solve Eq. (16) for substantially smaller number of measurements than for the direct reconstruction, that is, for M_{nm} being a rectangular matrix with $n \ll m$. In the compressive sensing process, only the most significant sparse coefficients of the representation are recovered.

The properties of the measurement matrix M_{nm} are fundamental to proper reconstruction [25]. Therefore, we construct M_{nm} from repeated random measurements and aim to satisfy the restricted isometry property and incoherence between measurements. The solution of (16) for $n \ll m$ is found through the matching pursuit algorithm [26], by requiring

$$\min \left\| y_n - \sum_m M_{nm} \hat{A}_m \right\|, \tag{18}$$

where $\hat{A}_m$ is found iteratively by computing the correlation vector at the j th iteration as

$$c_o^j = \sum_n M_{no}^* \left(y_n - \sum_m M_{nm} \hat{A}_m^j \right), \tag{19}$$

FIG. 5. The letter α reconstructed from a limited number of samples (given below the plots as percentages to three significant digits) in $\mathbf{k}$ space.

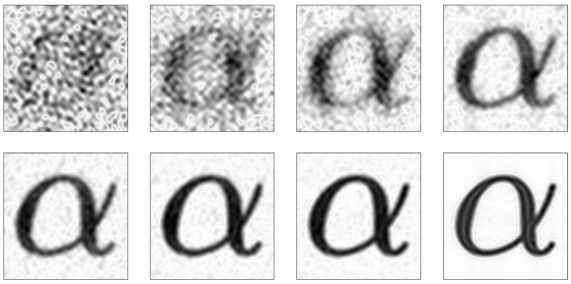

FIG. 6. Letters reconstructed by the compressive sensing approach by using (from top left) 25, 50, 100, 200, 300, 400, and 500 experiments. The last plot (lower right) shows the result of direct reconstruction (corresponding to 560 experiments).

and updating the current approximation to the sparse representation $\hat{A}_m^{j+1} = \hat{A}_m^{j+1} + c_s \delta_s$, where the index s maximizes the correlation (i.e., $\max_s |c_s|$). As a result, each iteration localizes and approximates a sparse coefficient in $\hat{A}_n$.

The results of the single-pixel reconstruction process for 25, 50, 100, 200, 300, 400, and 500 measurements with 15 harmonics are presented in Fig. 6. Compared to the direct image reconstruction that required 560 measurements, it can be seen that the letter can be clearly recognized using only 100 experiments (i.e. less than 20% of that data).

The possibility of recovering the image of an object from a single-point measurement is relevant for those fields where large arrays of detectors are expensive, as is the case for microwaves or acoustic waves, where the low frequency of the fields makes it more realistic to physically implement a time-modulated material or interface. In acoustical systems, the time-modulating elements can, for instance, be interfaces with variable transmission properties, such as cracks or delaminations under dynamic excitation [27]. Although advances have been made in the temporal modulation of materials in the optical domain, the excitation detection of a large enough number of harmonics to be able to perform perfect imaging for optical waves is still challenging [28]. Therefore, we consider that a realistic proposal for a realization of this imaging system should begin for low-frequency fields.

IV. SUMMARY

In summary, we have shown that a time-modulated grating can be used to overcome the diffraction limit for imaging in the far-field. It has been shown that placing two identical gratings between the object and the detector produces a field distribution from which we can recover the image of the object with virtually unlimited resolution, since the evanescent components of the image have been coupled to high-frequency harmonics by the first grating and decoupled by the second one. If the object

is axially symmetric, this method allows for the recovery of the image by analyzing the temporal spectra of the total field at a single point, therefore constituting a superresolution single-pixel imaging system. In the case of having nonsymmetric objects, the second time grating can be replaced by a spatially inhomogeneous screen, and the single-pixel recovery method works similarly. Finally, the theory of compressive sensing has been used to significantly reduce the amount of data required, and numerical experiments have been presented supporting our findings. This work shows that space-time gratings can work as ultrafast single-pixel perfect imaging devices, which opens the door to applications in optics and other domains where waves are used for imaging.

ACKNOWLEDGMENTS

Daniel Torrent acknowledges financial support through the Ramón y Cajal fellowship under Grant No. RYC-2016-21188 and to the Ministry of Science, Innovation and Universities through Project No. RTI2018-093921-A-C42. Pawel Packo acknowledges the support of the National Science Centre in Poland through Grant No. [2018/31/B/ST8/00753]. This research was supported in part by PLGrid Infrastructure and by the DYNAMO project (101046489), funded by the European Union. Views and opinions expressed are, however, those of the authors only and do not necessarily reflect those of the European Union or European Innovation Council. Neither the European Union nor the granting authority can be held responsible for them. Both authors acknowledge Steven Cummer, Jesús Lancis, Enrique Tajahuerce and Vicente Durán for useful and fruitful discussions.

[1] Joseph W. Goodman, *Introduction to Fourier optics* (Roberts and Company Publishers, 2005).
[2] Chiyan Luo, Steven G. Johnson, J. D. Joannopoulos, and J. B. Pendry, Subwavelength imaging in photonic crystals, Phys. Rev. B **68**, 045115 (2003).
[3] Francesco Simonetti, Multiple scattering: The key to unravel the subwavelength world from the far-field pattern of a scattered wave, Phys. Rev. E **73**, 036619 (2006).
[4] B. Wood, J. B. Pendry, and D. P. Tsai, Directed subwavelength imaging using a layered metal-dielectric system, Phys. Rev. B **74**, 115116 (2006).
[5] Satoshi Kawata, Atsushi Ono, and Prabhat Verma, Subwavelength colour imaging with a metallic nanolens, Nat. Photonics **2**, 438 (2008).
[6] Jie Zhu, Johan Christensen, Jesper Jung, Luis Martin-Moreno, X. Yin, Lee Fok, Xiang Zhang, and F. J. Garcia-Vidal, A holey-structured metamaterial for acoustic deep-subwavelength imaging, Nat. Phys. **7**, 52 (2011).
[7] Edward T. F. Rogers, Jari Lindberg, Tapashree Roy, Salvatore Savo, John E. Chad, Mark R. Dennis, and Nikolay I. Zheludev, A super-oscillatory lens optical microscope for subwavelength imaging, Nat. Mater. **11**, 432 (2012).
[8] Chu Ma, Seok Kim, and Nicholas X. Fang, Far-field acoustic subwavelength imaging and edge detection based on spatial filtering and wave vector conversion, Nat. Commun. **10**, (2019).
[9] Bakhtiyar Orazbayev and Romain Fleury, Far-field subwavelength acoustic imaging by deep learning, Phys. Rev. X **10**, 031029 (2020).
[10] Ari Sihvola, Metamaterials in electromagnetics, Metamaterials **1**, 2 (2007).
[11] Tie Jun Cui, David R. Smith, and Ruopeng Liu, *Metamaterials* (Springer, 2010).
[12] Nikolay I. Zheludev and Yuri S. Kivshar, From metamaterials to metadevices, Nat. Mater. **11**, 917 (2012).
[13] B. D. F. Casse, W. T. Lu, Y. J. Huang, E. Gultepe, L. Menon, and S. Sridhar, Super-resolution imaging using a three-dimensional metamaterials nanolens, Appl. Phys. Lett. **96**, (2010).
[14] Dylan Lu, Zhaowei Liu, Hyperlenses and metalenses for far-field super-resolution imaging, Nat. Commun. **3**, 1 (2012).
[15] Mohammadreza Khorasaninejad, Wei Ting Chen, Robert C. Devlin, Jaewon Oh, Alexander Y. Zhu, and Federico Capasso, Metalenses at visible wavelengths: Diffraction-limited focusing and subwavelength resolution imaging, Science **352**, 1190 (2016).
[16] Pooria Salami and Leila Yousefi, Far-field subwavelength imaging using phase gradient metasurfaces, J. Lightwave Technol. **37**, 2317 (2019).
[17] Victor Pacheco-Peña and Nader Engheta, Temporal aiming, Light: Sci. Appl. **9**, 1 (2020).
[18] Dani Torrent, Strong spatial dispersion in time-modulated dielectric media, Phys. Rev. B **102**, 214202 (2020).
[19] H. Nassar, H. Chen, A. N. Norris, and G. L. Huang, Non-reciprocal flexural wave propagation in a modulated metabeam, Extreme Mech. Lett. **15**, 97 (2017).
[20] Daniel Torrent, Olivier Poncelet, and Jean-Chirstophe Batsale, Nonreciprocal thermal material by spatiotemporal modulation, Phys. Rev. Lett. **120**, 125501 (2018).
[21] Yangyang Chen, Xiaopeng Li, Hussein Nassar, Andrew N. Norris, Chiara Daraio, and Guoliang Huang, Nonreciprocal wave propagation in a continuum-based metamaterial with space-time modulated resonators, Phys. Rev. Appl. **11**, 064052 (2019).
[22] Xiaohui Zhu, Junfei Li, Chen Shen, Xiuyuan Peng, Ailing Song, Longqiu Li, and Steven A. Cummer, Non-reciprocal acoustic transmission via space-time modulated membranes, Appl. Phys. Lett. **116**, 034101 (2020).
[23] Daniel Torrent, William J. Parnell, and Andrew N. Norris, Loss compensation in time-dependent elastic metamaterials, Phys. Rev. B **97**, 014105 (2018).
[24] H.-x. Li, M. Rosendo-López, Y.-f. Zhu, X.-d. Fan, D. Torrent, B. Liang, J. Cheng, and J. Christensen, Ultra-thin acoustic parity-time symmetric metasurface cloak, Research **2019**, (2019).
[25] Richard G. Baraniuk, Compressive sensing [lecture notes], IEEE Signal Process. Mag. **24**, 118 (2007).
[26] S. G. Mallat and Zhifeng Zhang, Matching pursuits with time-frequency dictionaries, IEEE Trans. Signal Process. **41**, 3397 (1993).

[27] J. Rivière, M. C. Remillieux, Y. Ohara, B. E. Anderson, S. Haupert, T. J. Ulrich, and P. A. Johnson, Dynamic acousto-elasticity in a fatigue-cracked sample, J. Nondestruct. Evaluation **33**, 216 (2014).

[28] E. Galiffi, R. Tirole, S. Yin, H. Li, S. Vezzoli, P. A. Huidobro, M. G. Silveirinha, R. Sapienza, A. Alu, and J. B. Pendry, Photonics of time-varying media, Adv. Photon. **4**, (2022).